

Understanding complex magnetic order through analyses of local atomic structure

James R. Neilson* and Daniel E. Morse†
Biomolecular Science & Engineering
University of California Santa Barbara, CA 93106

Brent C. Melot, Daniel P. Shoemaker, Joshua A. Kurzman, and Ram Seshadri
Materials Department and Materials Research Laboratory
University of California Santa Barbara, CA 93106

(Dated: July 19, 2022)

In many ostensibly crystalline materials, unit-cell-based descriptions do not always capture the complete physics of the system due to interruption of long-range order. In the series of cobalt hydroxides studied here, magnetic Bragg diffraction reveals a fully compensated Néel state, yet the materials show significant and open magnetization loops. A detailed analysis of the local structure defines the aperiodic arrangement of cobalt coordination polyhedra. Representation of the structure as a combination of distinct polyhedral motifs explains the existence of locally uncompensated moments and provides a quantitative agreement with bulk magnetic measurements and magnetic Bragg scattering.

PACS numbers: 75.25.-j, 61.66.-f, 64.60.Cn, 61.66.Fn

Complex magnetic ground states in crystalline materials frequently derive from the details of the underlying lattices. In the popular example of insulating compounds where the magnetic ions arrange themselves with three-fold symmetries (*e.g.* triangular or pyrochlore lattices), geometric frustration of magnetic interactions prevent magnetic ordering or give rise to exotic ground states [1]. Alternatively, the dilution of magnetic ions can give rise to complex magnetic order, since the translational periodicity of the lattice is necessarily interrupted.

For example, in diluted uniaxial anisotropic antiferromagnets, such as $\text{Co}_{1-x}\text{Zn}_x\text{F}_2$, local uncompensated moments result from random variations in the exchange interactions from the non-magnetic impurities [2]. Upon zero-field cooling, diffraction reveals a Néel state; however, the random fields decrease the diffracted peak intensity from disrupted long-range order (LRO) and field cooling completely destroys the LRO [3, 4]. Because these systems show no preference for chemical or short-range order within a disordered nuclear unit-cell [4], it is difficult to structurally distinguish the role of the impurities in establishing the random fields and microdomains.

In the layered α -cobalt hydroxides studied here, we propose that chemical short-range order of the local structure generates similar complex magnetic behavior. The series of cobalt hydroxide chlorides are described by the chemical formula $\text{Co}(\text{OH})_{2-x}(\text{Cl})_x(\text{H}_2\text{O})_n$, where $x = 0.0, 0.2, 0.3,$ and 0.4 approximate the tetrahedrally coordinated cobalt content [5]. In a traditional unit-cell based description of the structure, all cobalt site occupancies (g) are reduced ($g_{\text{oct}} = 1 - g_{\text{tet}}$) and incoherently averaged [Fig. 1(a)]. Therefore, a local description is needed locate all of the atom positions and occupancies. From our extensive analysis of the X-ray pair distribution functions of these compounds [6], the distribution of cobalt polyhedra is best described by an incoherent combination of structural motifs [Fig. 1(c-e)] schematically represented in Fig. 1(f). Magnetic susceptibility measurements

reveal uncompensated magnetization, but magnetic neutron diffraction suggests a periodic Néel antiferromagnetic structure. We present a method of assembling local motifs in real space to microscopically reconcile a quantitative description of the random distribution of exchange interactions and the resulting microdomains.

The experimental samples with $x = 0.2, 0.3, 0.4$ were prepared and characterized as previously described [5, 6] and material with $x = 0.0$ was purchased from Alfa-Aesar. Magnetic characterization was performed on powder samples embedded in paraffin wax (melted to 55°C) using a Quantum Design MPMS SQUID magnetometer. All other experimental procedures are described in the text or Supplemental Information.

The temperature dependent magnetic susceptibility (Fig. 2) reveals a systematic relationship with composition when non-dimensionalized by Curie-Weiss constants, $C/(\chi|\Theta_{\text{CW}}|) + \text{sgn}(\Theta_{\text{CW}}) = T/(|\Theta_{\text{CW}}|)$, obtained from a linear fit to $1/\chi = (T - \Theta_{\text{CW}})/C$ in the paramagnetic regime (200 K to 300 K) [7]. The unnormalized data are shown in the Supplemental Information. Generally, all of the cobalt hydroxides show strong deflections at $T/|\Theta_{\text{CW}}| = 1$, indicative of a magnetic phase transition. All the compounds studied also show small deviations as $T/|\Theta_{\text{CW}}|$ approaches unity on cooling. These are compensated short-range spin interactions if above the ideal Curie-Weiss relationship, or uncompensated when below [7]. The β - $\text{Co}(\text{OH})_2$ compound ($x = 0$) shows that compensated interactions arise when $T/|\Theta_{\text{CW}}| > 1$, attributable to the longer-range ($\propto r^{-3}$) interlayer dipolar exchange, which is also observed when the layers become decorated with tetrahedra ($x = 0.2$); however, uncompensated interactions emerge when $x > 0.2$. This crossover is reflected in Θ_{CW} , which is positive (ferromagnetic) for $x \leq 0.2$, and negative (antiferromagnetic) as $x > 0.2$. As x increases for $x > 0.0$, $|\Theta_{\text{CW}}|$ decreases below T_c , suggesting a decrease in the interaction strength. From a mean-field perspective, we interpret this to indicate that the dominant interaction switches from in-

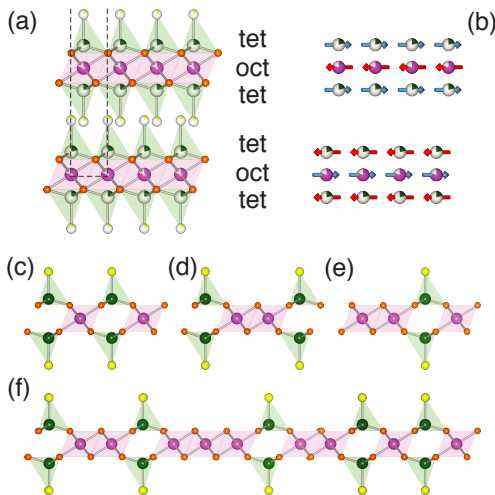


FIG. 1: (a) Average structure of layered cobalt hydroxide chloride displaying two layers of a half of a unit-cell (dashed line) and fractionally occupied (partially filled) metal sites. (b) Symmetry allowed spin arrangement deduced from neutron scattering and (c-e) the locally ordered distributions of capping tetrahedral Co^{2+} , with ratios of 2 Co^{tet} per (c) 3 Co^{oct} , (d) 8 Co^{oct} , and (e) 15 Co^{oct} . (f) Schematic representation of a single layer of cobalt hydroxide chloride from a pair distribution function analysis [6]. Pink spheres denote Co^{oct} , green Co^{tet} ; oxygen is orange, chlorine yellow. (color online)

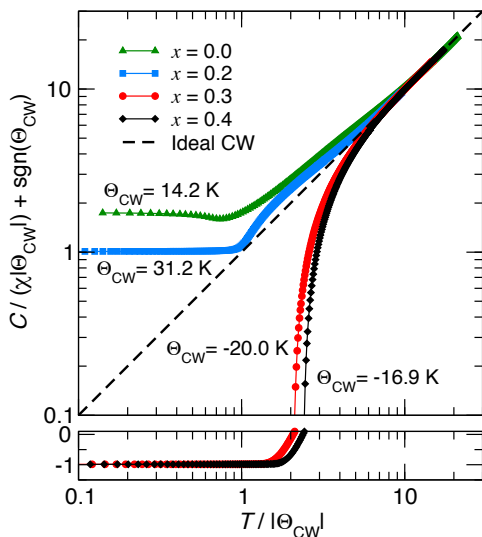


FIG. 2: Temperature dependent scaled inverse susceptibility of $\text{Co}(\text{OH})_{2-x}(\text{Cl})_x(\text{H}_2\text{O})_n$ for $x = 0.0, 0.2, 0.3,$ and 0.4 , illustrating positive compensated and negative uncompensated deviations from ideal Curie-Weiss paramagnetism. (color online)

tralayer ferromagnetic coupling when $x \leq 0.2$, as found in all-octahedrally coordinated cobalt(II) compounds [8], to antiferromagnetic interactions between distinct polyhedra.

The isothermal magnetization (2 K, Fig. 3) of $x = 0$ is indicative of antiferromagnetic order with a spin-flop transition [8, 9]. The hysteresis loops open when $x > 0$ with a coordination independent saturation magnetization at $1.1\text{-}1.2 \mu_{\text{B}} \text{mol}^{-1}$

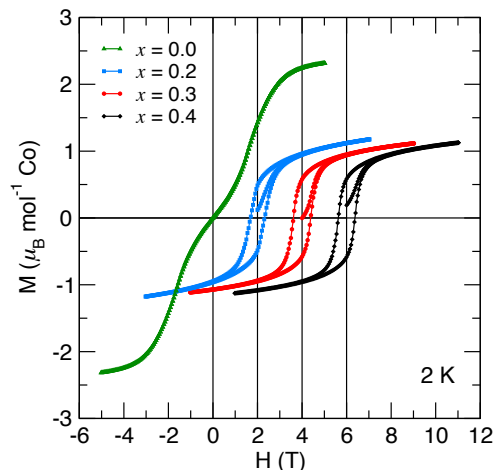


FIG. 3: Isothermal magnetization of $\text{Co}(\text{OH})_{2-x}(\text{Cl})_x(\text{H}_2\text{O})_n$ for $x = 0.0, 0.2, 0.3,$ and 0.4 at 2 K showing the composition independent saturation magnetization for $x > 0.0$. The inflection point in the initial magnetization indicates a weak field induced transition. Each curve is offset by 2 T for clarity. (color online)

Co (Obs. M_{sat} in Table I). This contradicts previous studies on similar structure types [10] which calculate the magnetization from the different number of spins on one Néel sublattice (Co^{oct}) to the other (Co^{tet}): Néel $M_{\text{sat}} = 3/2(\text{Co}^{\text{oct}} - \text{Co}^{\text{tet}})$. In that spin arrangement, one expects a coordination dependent magnetization (Table I, Néel M_{sat}).

Further elucidation of the temperature dependent magnetism is provided with the magnetic specific heat for each compound, determined using non-magnetic analogs, $\text{Mg}(\text{OH})_2$ for $\beta\text{-Co}(\text{OH})_2$ and $\text{Zn}(\text{OH})_{1.6}(\text{Cl})_{0.4}(\text{H}_2\text{O})_{0.2}$ for $\alpha\text{-Co}(\text{OH})_2$, after appropriately scaling the temperature axes for differences in mass [11], to independently isolate the magnetic contribution to the heat capacity [20]. The low temperature exponents (T^β , Table I) resemble those of two-dimensional magnetic systems, indicating weak interlayer coupling [12]. The total entropy lost through the transition is only 25% of the expected value for full ordering of a $S = 3/2$ system [$\Delta S = R \ln(2S + 1)$] for $x > 0$ (Fig. 4, Table I). Thus, spin disorder appears to persist even at 2 K. Thus, we identify any periodic magnetic order using neutron diffraction.

Magnetic Bragg scattering from time-of-flight neutron powder diffraction of $\text{Co}(\text{OD})_{1.6}(\text{Cl})_{0.4}(\text{D}_2\text{O})_{0.3}$ ($x = 0.4$; Fig. 5) indicates a Néel antiferromagnetic structure [Fig. 1(b)] [21]. Below the magnetic ordering temperature, we observe only the appearance of broad Bragg reflections at $d = 3.20 \text{ \AA}$, 5.35 \AA , and 16.31 \AA [Fig. 5(b)], corresponding to an incommensurate magnetic propagation vector of $\mathbf{k} = (0, 0, 1.5)$. Examination of the diffuse scattering backgrounds at 300 K and 6 K do not show evidence for short-range spin correlations. Using PDFGETN [13] to account for sample absorption, and FULLPROF [14] and BASIREPS [15] to refine the profile across multiple detector banks (14° , 40° , and 90°), we identified a unique irreducible representation (Γ_6 , Supplemental

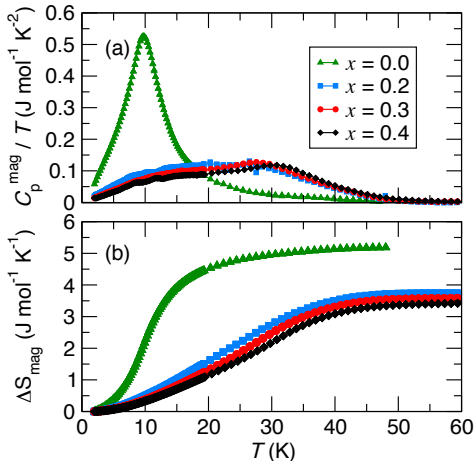


FIG. 4: (a) Temperature normalized magnetic heat capacity $[(C_p - C_{\text{lattice}})/T]$ as a function of temperature indicating a broad hump centered around T_c for all compounds. (b) Entropy release through the magnetic ordering transition illustrating the remainder of spin disorder down to 2 K and large entropy losses above the magnetic transition temperature. (color online)

Information) with two equivalent sets of basis vectors capable of reproducing the magnetic peaks. However, powder and domain averaging precludes determination of a unique orientation of the basis vectors within the ab plane. The average magnetic structure, illustrated in Fig. 1(b), describes a spin arrangement with in-plane ferromagnetically coupled spins on octahedral cobalt sites that are antiferromagnetically aligned to adjoining tetrahedral sites. Each layer is antiferromagnetically coupled, yielding a fully compensated magnetic structure, inconsistent with the observed behavior.

Rietveld refinement of the nuclear positions reveals reasonable atomic displacements for the magnetic nuclei, but a large degree of static disorder for the interlayer species (Supplemental Information, Ref. 6). While the cobalt positions are well-defined, refinement to the magnetic reflections ($R_{\text{mag}} = 14.8\%$, 14° detector bank) reveals partial spin disorder. The basis vector Fourier coefficients indicate reduced moments of both cobalt sites: $1.2 \mu_B$ for Co^{oct} , and $1.1 \mu_B$ for Co^{tet} . The magnetic reflections also have a significantly increased Lorentzian breadth, which in combination with the reduced moment, resembles the reduced spin ordering from a microdomain state from random fields [3, 4, 16]. Here, the microdomains result not from magnetic ion dilution, but rather the local clustering of polyhedra.

To reconcile ambiguities engendered from fractional occupancy in the unit-cell, we refer to our previous local structure study of the pair distribution functions of layered cobalt hydroxide chlorides [6], depicted in Fig. 1(c-f). We represent the structure from a distribution of $[\text{Co}_n^{\text{oct}}\text{Co}_2^{\text{tet}}]$ motifs with a set number of octahedra between tetrahedra. These incoherently distributed motifs serve as the microdomains for describing the observed magnetic behavior. Microscop-

TABLE I: Expected saturation magnetization assuming a two-sublattice Néel model, saturation magnetization for an explicit treatment of the local structure, and the observed magnetization (2 K, 5 T) for each compound ($x = 0.0, 0.2, 0.3, 0.4$) [6]. Summary of the magnetic heat capacity measurements: lost entropy and temperature exponent at $T \ll T_c$.

x	Néel	Local	Obs.	Heat capacity	
	M_{sat}	M_{sat}	M_{sat}	ΔS_{mag}	β
		$(\mu_B \text{ mol}^{-1} \text{ Co})$		$(\text{J mol}^{-1} \text{ K}^{-1})$	(T^β)
0.0	n/a	n/a	2.3	5.2	2.0
0.2	0.9	1.14	1.2	3.7	1.9
0.3	0.6	1.14	1.1	3.6	2.0
0.4	0.3	1.13	1.1	3.4	2.3

ically, the $[\text{Co}_3^{\text{oct}}\text{Co}_2^{\text{tet}}]$ and $[\text{Co}_8^{\text{oct}}\text{Co}_2^{\text{tet}}]$ domains, illustrated in Fig. 1(c,d), consist of ferromagnetically coupled spins between edge shared octahedra, but tetrahedral sites remain disordered at low temperatures. However, in $[\text{Co}_{15}^{\text{oct}}\text{Co}_2^{\text{tet}}]$ motifs [Fig. 1(e)], spins on tetrahedral coordinated cobalt ions order antiferromagnetically to the octahedra.

The presence of defect spins, as from tetrahedrally coordinated cobalt sites, often leads to spin disorder. When defect spins are placed adjacent to well-ordered ferromagnetic layers, as seen in layered $(1-x)\text{FeTiO}_3-x\text{Fe}_2\text{O}_3$ solid solutions [17], exotic ground states involving canted or spiral spin structures are stabilized [18]. Here, the strong magnetocrystalline anisotropy of octahedral Co^{2+} [19] prevents the canting of spins from the crystal field axes, giving them an Ising character. Competition between the dominant ferromagnetically coupled layers and the magnetocrystalline anisotropy prevents the formation of a well-ordered ground state for high concentrations of defect tetrahedral Co^{2+} spins, supporting the observed trend in decreasing magnetic entropy release with increasing Co^{tet} sites.

While Goodenough-Kanamori-Anderson superexchange considerations suggest a preference for antiferromagnetic coupling between distinct polyhedra, this interaction is weak, as indicated from the sign change and decreasing $|\Theta_{\text{CW}}|/T_c$ with increasing x . On average, a small fraction of tetrahedral spins must align antiparallel to the octahedra, as determined from magnetic neutron diffraction by the magnetic propagation vector and a 12% reduced refined moment on the tetrahedral sites relative to the octahedra. Glassy tetrahedral spins disrupt the coherence of interlamellar dipolar coupling, permitting a low field spin-flop transition. This is observed in the initial magnetization by a change in curvature in $M(H)$ at ~ 0.4 T (Fig. 3). As the field is reversed, proximal Néel ordered Co^{tet} spins from neighboring layers couple *via* dipolar interactions along the interlayer space, preventing immediate reversal of the field induced transition. This gives rise to a remanent magnetization (Fig. 3) and a large frequency dependent amplitude and phase in $\chi(\omega, T)$ (Supplemental Information). While the disparity between the observed magnetization and the fully compensated average Néel antiferromagnetic structure can be reconciled with a spin flop transition,

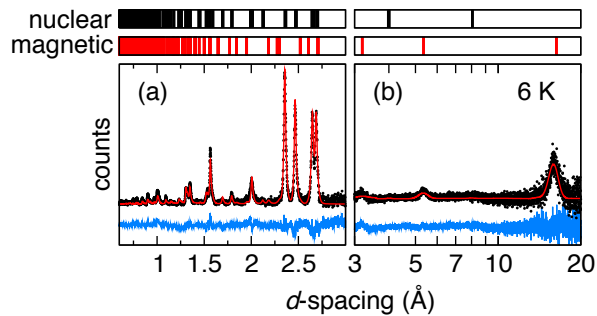


FIG. 5: Time-of-flight powder neutron diffraction (HIPD, LANL) of $\text{Co}(\text{OD})_{1.6}(\text{Cl})_{0.4}(\text{D}_2\text{O})_{0.3}$ at 6 K (black dots) from (a) 90° and (b) 14° detector banks showing Bragg planes of the nuclear (black hashes) and magnetic [red hashes, $\mathbf{k} = (0, 0, 1.5)$] phases with the Rietveld refined profile (red line) above the difference curve (blue line). (color online)

this cannot account for the nearly composition independent constant saturation magnetization, T_c , and entropy release. Therefore, a local analysis of the structure must be applied to reconcile these differences.

From the polyhedral composition provided by the real-space analysis [6], we calculate the individual moment contributions from each local moiety with the assumption that all Co^{oct} are parallel, and dilute Co^{tet} spins (as in $[\text{Co}_{15}^{\text{oct}}\text{Co}_2^{\text{tet}}]$) are antiparallel to Co^{oct} in a Néel configuration. Letting A , B , and C represent the atomic phase fractions (Supplemental Information) of the local moieties provided from Ref. 6 for $[\text{Co}_3^{\text{oct}}\text{Co}_2^{\text{tet}}]$, $[\text{Co}_8^{\text{oct}}\text{Co}_2^{\text{tet}}]$, $[\text{Co}_{15}^{\text{oct}}\text{Co}_2^{\text{tet}}]$, respectively, the summed moment from each microdomain is calculated as:

$$M_{\text{sat}} = \frac{3}{2} \left(\frac{3A + 8B + (15 - 2)C}{5A + 10B + 17C} \right) \quad (1)$$

Using Eq. 1, the locally derived saturation moments for $x = 0.2, 0.3,$ and 0.4 are tabulated in Table I (Local M_{sat}). We compute a negligible dependence of M_{sat} on composition with values comparable to those observed. The agreement of the observed properties with the assembly of local contributions reconciles the inaccuracies resulting from the disordered average structure and microdomain-like magnetic diffraction.

While the average symmetry-allowed magnetic structure appears as a fully compensated Néel-type antiferromagnet, the magnetic behavior is better explained by local and incoherent intralayer Néel ferrimagnetic regions that become aligned with an applied field, interspersed with disordered defect spins that interrupt compensation of the ferrimagnetic regions from layer to layer. We present an extreme case where magnetic site occupancy exhibits no long-range order, yet a long-range ordered magnetic structure is observed, on average. In systems where incoherent disorder is present, average methods operate under the assumption that a single unit-cell is sufficient. We illustrate here that the local atomic structure offers an alternative structural mechanism for introducing random fields in a

magnetic lattice to yield microdomain behavior.

JRN gratefully thanks the NSF for support through the Graduate Research Fellowship. The authors thank E.E. Rodriguez and T.M. McQueen for helpful discussions. JAK thanks the ConvEne-IGERT Program (NSF-DGE 0801627) for an Associateship. This research was supported by a grant from the DOE, Office of Basic Energy Science to DEM (DEFG03-02ER46006) and to JAK (DE-FG02-10ER16081); and by use of the time-of-flight beam line HIPD at DOE's Lujan Center at Los Alamos National Laboratory (operated by Los Alamos National Security, LLC under DOE under Contract No. DE-AC52-06NA25396), and UCSB's Materials Research Laboratory (MRL) Central Facilities, supported by the MRSEC Program (NSF, Award No. DMR05-20415), to which BCM also acknowledges financial support; the MRL is a member of the NSF-funded Materials Research Facilities Network (www.mrfln.org).

* Electronic address: neilson@lifesci.ucsb.edu

† Electronic address: d.morse@lifesci.ucsb.edu

- [1] A. P. Ramirez, *Annu. Rev. Mater. Sci.* **24**, 453 (1994).
- [2] S. Fishman and A. Aharony, *J. Phys. C* **12**, L729 (1979).
- [3] H. Yoshizawa, R. A. Cowley, G. Shirane, R. J. Birgeneau, H. J. Guggenheim, and H. Ikeda, *Phys. Rev. Lett.* **48**, 438 (1982).
- [4] M. Hagen, R. A. Cowley, S. K. Satija, H. Yoshizawa, G. Shirane, R. J. Birgeneau, and H. J. Guggenheim, *Phys. Rev. B* **28**, 2602 (1983).
- [5] J. R. Neilson, B. Schwenzer, R. Seshadri, and D. E. Morse, *Inorg. Chem.* **48**, 11017 (2009).
- [6] J. R. Neilson, J. A. Kurzman, R. Seshadri, and D. E. Morse, *Chem. Eur. J.* **16**, 9998 (2010).
- [7] B. C. Melot, J. E. Drewes, R. Seshadri, E. M. Stoudenmire, and A. P. Ramirez, *J. Phys.: Condens. Matter* **21**, 216007 (2009).
- [8] P. Rabu, S. Angelov, P. Legoll, M. Belaiche, and M. Drillon, *Inorg. Chem.* **32**, 2463 (1993).
- [9] T. Takada, Y. Bando, M. Kiyama, and H. Miyamoto, *J. Phys. Soc. Japan* **21**, 2726 (1966).
- [10] M. Kurmoo, *Phil. Trans. R. Soc. Lond. A* **357**, 3041 (1990).
- [11] A. Tari, *The Specific Heat of Matter at Low Temperatures* (Imperial College Press, 2003).
- [12] L. P. Regnault and J. Rossat-Mignod, in *Magnetic Properties of Layered Transition Metal Compounds*, edited by L. J. de Jongh (Kluwer Academic Publishers, 1990).
- [13] P. F. Peterson, M. Gutmann, T. Proffen, and S. J. L. Billinge, *J. Appl. Crystallogr.* **33**, 1192 (2000).
- [14] J. Rodriguez-Carvajal, *Physica B* **192**, 55 (1993).
- [15] J. Rodriguez-Carvajal, *Mater. Sci. Forum* **378-381**, 268 (2001).
- [16] R. J. Birgeneau, H. Yoshizawa, R. A. Cowley, G. Shirane, and H. Ikeda, *Phys. Rev. B* **28**, 1438 (1983).
- [17] Y. Ishikawa, *J. Phys. Soc. Jpn.* **17**, 1835 (1962).
- [18] A. C. Berceanu, Master's thesis, University of Groningen (2008).
- [19] J. Kanamori, *Prog. Theor. Phys.* **17**, 197 (1957).
- [20] Measured with a semi-adiabatic technique using a Quantum Design Physical Properties Measurement System (PPMS)
- [21] Diffraction recorded at the time-of-flight beam line HIPD at Los Alamos National Laboratory at 300 K and 6 K.